Fracture Behavior Characterization of Arcan Polycaprolactone Based Polymer Composites Prepared by Polymerization Induced Phases Separation

Pengfei Zhang,[1] **Ziyao Gao**,[2] **Qian Zhang**,[3] **Ahmed Khattab**,[1] **Guoqiang Li**[4]
[1]*Department of Industrial Technology, College of Engineering, University of Louisiana at Lafayette, Lafayette, Louisiana, 70504*

[2]*Department of Mechanical Engineering, College of Engineering, University of Louisiana at Lafayette, Lafayette, Louisiana, 70504*

[3]*Department of Civil Engineering, College of Engineering, University of Louisiana at Lafayette, Lafayette, Louisiana, 70504*

[4]*Department of Mechanical and Industrial Engineering, Louisiana State University, Baton Rouge, Louisiana, 70803*

Polycaprolactone (PCL) based polymer composites have several potential engineering applications. This study investigated the fracture toughness of polycaprolactone based polymer composites under mode I, mode II, and mixed mode I&II, according to the use of Arcan composite specimens. The specimen was prepared through a polymerization-induced phase separation (PIPS) process by diffusing polycaprolactone within an epoxy matrix. The thermal properties and morphology of the specimen fracture surfaces were characterized firstly. After that shape memory performance of the prepared specimen was preliminarily studied by measuring the recovered strain and stress. Specimens were tested under compression according to ASTM D6641. Arcan specimens used in this study for studying the fracture behavior under different fracture modes were prepared using a Waterject. The effect of loading angles on the fracture behavior was investigated as well. The results show that Arcan specimen has advantages on studying the fracture behavior of polycaprolactone based polymer composite under different fracture modes. It found that the average size decreases as the amount of PCL increasing. The globules are uniformly distributed across the fracture surfaces. The shape memory test shows that the larger programmed strain the larger recovered stress. In addition, the increase of PCL amount leads to the decrease of composite K_{IC} but the increase of K_{IIC} (i.e., improved shear resistance). We envision application of the developed Arcan test fixture as a testing device to exam the crack healing efficiency under different fracture modes. POLYM. COMPOS., 40:1198–1208, 2019. © 2018 Society of Plastics Engineers

Correspondence to: P. Zhang; e-mail: pzhang@louisiana.edu
Contract grant sponsor: College of Engineering at the University of Louisiana at Lafayette; contract grant number: 210125.
DOI 10.1002/pc.24831
Published online in Wiley Online Library (wileyonlinelibrary.com).

INTRODUCTION

Polycaprolactone (PCL) based polymer composites have found many potential applications in lightweight structures [1–8]. One such application is self-healing composite structures based on shape memory effect (SME). In the so called close-then-heal (CTH) strategy [9], shape recovery force has been used to close wide opened cracks, and either intrinsic or extrinsic healing strategies have been used to heal the closed cracks. This can be further divided into two categories. One is based on compression programmed shape memory polymer matrix. Constrained shape recovery (expansion) of the shape memory polymer (SMP) matrix helps close cracks in the composite [10, 11]. The other is based on non-shape memory, conventional polymer matrix embedded with tension programmed SMP fibers [12] or polymeric artificial muscles [13]. Constrained shape recovery of the SMP fiber or polymeric artificial muscle (shrinkage) helps close the wide opened cracks. In order to evaluate the healing efficiency, various approaches have been used such as compression after impact [14–16], single-notched beam bending [17, 18], single-notched beam tension [19], and tapered double cantilever beam (TDCB) fracture tests

[20–22]. Fracture test is preferred because it is an energy based approach, measuring the energy release rate as well as cohesive traction-separation behavior, and is more comprehensive to measure the healing efficiency. In real world structures, however, various fracture modes are involved, including mode I, mode II, and mixed mode I&II. While TDCB specimens can measure the mode I fracture resistance, mode II and mixed mode I&II measurement are highly desired to evaluate the healing efficiencies.

Various types of specimens have been used in fracture tests such as double cantilever beam (DCB) test for mode I (opening), end-notched flexure (ENF) for mode II (shear), and the crack rail shear (CRS) for mode III (tearing) [23, 24]. In real world structures, the fracture modes are usually mixed modes. Many test methods have been developed to characterize the fracture behaviors under mixed-mode loading conditions, such as the mixed-mode flexure (MMF), end loaded split (ELS), single leg bending (SLB), crack lap shear (CLS), edge delamination tension (EDT), asymmetric double cantilever beam (ADCB), and mixed-mode bending (MMB) [25]. However, they involve different types of specimens or test configurations, which would introduce different test variables and analysis procedures. As a result, it is difficult to predict fracture behavior of materials. The Arcan specimen was proposed to solve this issue, characterizing fracture toughness for mode I, mode II, mode III, and any combination of mode I/II and mode I/III with the same test configuration [26–28]. Arcan specimens enable the effect of load angles on fracture. By changing the loading angles or specimen types, different fracture modes could be tested. Therefore, Arcan specimens would be an ideal candidate for evaluating the healing efficiency of SMP composites under difference fracture modes or mode combinations.

A particulate polymer composite was prepared by dispersing 10% (by volume) PCL particles within resin matrix [18]. It proved that the polymer composite exhibited excellent repeatable crack healing performance. Two types of triple shape memory composites (TSMC) were developed by incorporating epoxy and poly(ε-caprolacton) via polymerization induced phase separation process [29]. The first TSMC of polypropylene glycol-epoxy/poly(ε-caprolacton) was prepared by reacting diglycidyl ether of bisphenol-A (DGEBA) and neopentyl glycol diglycidyl ether (NGDE) with poly(propylene glycol) bis(2-aminoprogyl ether) (Jeffamine D230) cross-linker in the presence of dissolved PCL (10 wt%). The second epoxy-based TSMC of polyethylene oxide-epoxy/poly (ε-caprolacton) was prepared by reacting DGEBA and *O,O'*-bis(2-aminopropyl) polypropylene glycol-block-polyethylene glycol-block-polypropylene glycol (Jeffamine ED2000) cross-linker in the presence of PCL (10 wt%). The results showed the ability of both types to fix two separate deformations independently and be able to recover both programmed shapes separately upon heating. In this study, polymer composites are prepared via polymerization-induced phase separation (PIPS) process, by diffusing PCL within an Epon epoxy matrix. The objectives here include:

- To develop an Arcan test fixture for polymer composites;
- To prepare shape memory polymer composite via polymerization induced phase separation process;
- To characterize the compression behavior and shape memory behavior of the prepared polymer composites;
- To evaluate the developed Arcan test fixture for characterizing the toughness of PCL based polymer composites.

Before testing the crack self-healing performance, the focus in this study is to develop an Arcan test fixture and study the sample fractural behavior under various modes. Shape memory behavior was preliminarily tested to prove its shape memory effect. In addition to shape recovery tests and compression tests, fractures tests in terms of Mode I, Mode II, and mixed Mode I&II were conducted per the Arcan specimens. The test results were analyzed and discussed, including fracture surface morphology, shape memory behavior, mechanical properties such as fracture toughness, as a function of PCL volume fraction. We envision application of the developed Arcan test fixture as a testing device to exam the crack healing efficiency under different fracture modes.

EXPERIMENTAL

Raw Materials

Perstorp CAPA 6500 PCL pellet, a high molecular weight thermoplastic linear polyester derived from caprolactone monomer, was used here to be mixed with matrix materials. It has a density of 1.14 g/cm^3 and melting temperature 58–60°C. The matrix material is the DPL 862 epoxy resin, which was cured with the triethylenetetramine (TETA) curing agent.

Composite Fabrication

Open mold with size of 304.8 mm × 55.88 mm × 12.7 mm was prepared for specimen fabrication. In this study, the amount of PCL within the Epoxy matrix is varied according to the percentages by volumes (PBV), which are 10%, 12%, and 14%. The PCL particles and epoxy resin were weighed according to the designed PBV and poured in a glass beaker. At the same time, the glass beaker was heated using a hot plate. Stirring started once the PCL particles were completely melted. The stirring process continued for 35 minutes. After that, it was cooled down in a waterbath for adding resin hardener. If the resin hardener was added at a temperature higher than 40°C, the curing process was fast, leading to fast increase in viscosity, which made the mixture difficult to be poured into the prepared mold. The hardener was added to the mixture once it was cooled down to 30°C. Then mixing was conducted with the hardener for 3 minutes.

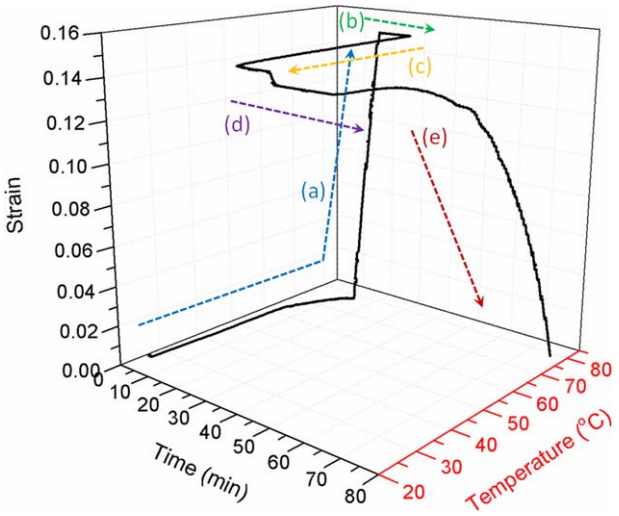

FIG. 1. Programming and strain recovery process in terms of temperature and time: (a) heating above the shape switch temperature and afterward loading; (b) maintaining the load; (c) cooling to the room temperature; (d) unloading; and (e) strain recovery upon heating. [Color figure can be viewed at wileyonlinelibrary.com]

The mixture was poured into the mold and kept at room temperature for complete curing. Cured panel was taken out from the mold after at least three days for sample cutting.

Thermal Property Test

Differential scanning calorimetry (DSC) testing was performed to characterize the thermal properties of the PCL based composite. The equipment used in this study was the SETARAM DSC 131 (Caluire, France). A hand file was used to scratch solid material into powder. Then the powder sample (with amount of 15.9 mg) was sealed within an aluminum pan. Three heating/cooling cycles were performed for this test, within the temperature range 18.44°C to 217.38°C. Air was used as purging gas.

Shape Recovery Tests

This test is to preliminarily verify the shape memory effect of prepared composite samples through PIPS. In order to test the shape recovery performance, an external load was applied onto the SMP to generate a temporary shape. After the programming process, tests on strain recovery or stress recovery were conducted to investigate the shape memory behavior. Thermal treatments were conducted, which included two parts: (1) thermal programming and (2) thermal recovery. The programming process enables specimens to gain temporary configuration; while the recovery process records the recovered stress or strain. Figure 1 shows a typical thermal programming and thermal recovery process for shape memory material: (a) provide heat first and then load; (b) hold the load at the programming temperature; (c) cool down to a lower temperature while keeping the load; (d) remove the load; and (e) provide heat again for shape recovery.

In this study, specimens were programmed at a temperature of 80°C. The specimens were put in an oven which was heated at a rate of 1.8°C/min. Once it reached the programming temperature, it was maintained for 10 minutes to make sure that specimens were completely heated up. After that, the specimens were uniaxially compressed to a strain of 0.13. Then it was cooled down to room temperature while keeping the applied load. Shape memory performance can be investigated either through stress recovery or strain recovery.

Compression Tests

The prepared composites were cut into samples with size of 25.4 mm × 25.4 mm × 12.7 mm for compression tests. Compression tests were carried out using an MTS Alliance RF/100 device with a 100 kN load cell, according to the ASTM D6641. Three samples were prepared for each test. Small displacement in the elastic region was measured using the Digital Image Correlation (DIC). Howeve, larger displacement was collected through the testing crosshead. The specimens were painted plain white and then black paint was used to create randomly distributed fine speckles on the white background. Digital images were captured by using a high resolution single-lens reflex Nikon camera during the loading. The captured images were input into commercial software packages (i.e., VIC-2D) to obtain full-field 2-D strain information based on the relative displacements between the speckles.

Fracture Tests

Waterjet was used to machine test specimens according to the geometry shown in Fig. 2. This allows Arcan specimens with precise sizes. In Fig. 2, a is the crack length, W is the specimen width, and t is the specimen thickness. θ is an angle between the sample axial direction and loading direction. Rotating the circular holder and connecting the circular holder to gripper by inserting pin to other available holes can change the θ from 0° to 90°. The notch was firstly cut by a diamond metal bond wafering blade (Allied High Tech Products, Inc, CA). The blade thickness is 0.51 mm. The cutting edge is round with radius 0.25 mm. Consequently, the pre-notch tip is round due to the used cutting blade. In order to have a sharp notch, a razor blade was used and slid in one motion across the notch root. The depth of the razor notch generated by sliding the razor blade was two times longer than the width of the pre-notch tip radius. The total size of pre-crack was determined according to the ratio a/W that is 0.2, 0.4, and 0.6. If the sample is cut like the one shown in Fig. 2, in the case of $\theta = 0°$, the loading direction is parallel with the sample axial direction, which means the test is under crack opening Mode I

 DOI 10.1002/pc

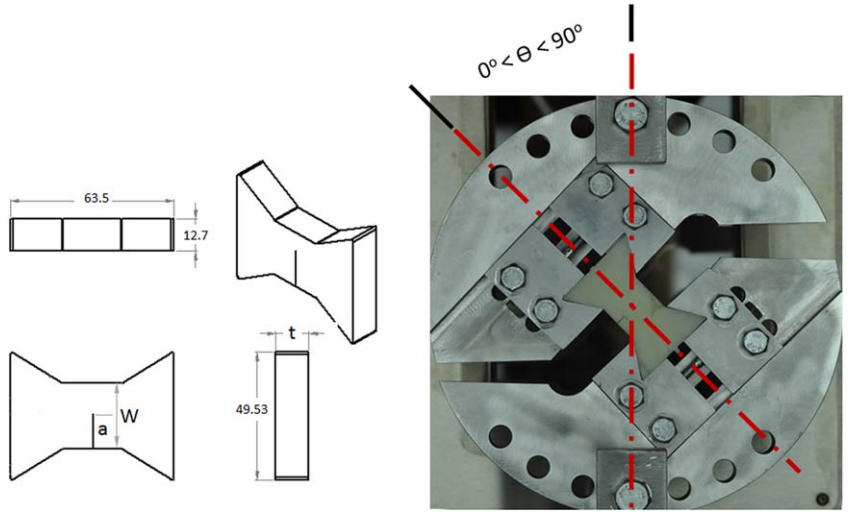

FIG. 2. Tested specimen geometry and fracture test fixture. [Color figure can be viewed at wileyonlinelibrary.com]

fracture; in the case of $\theta = 90°$, the loading direction is perpendicular to the sample axial direction, suggesting that the test is under in-plane shearing Mode II fracture; in the case of $0° < \theta < 90°$, the test sample is undergoing mixed crack opening and in-plane shearing, suggesting the test is under mixed Mode I&II fracture. Three samples were prepared for each test.

Scanning Electron Microscopy

JEOL JSM-6300 field emission scanning electron microscopy (SEM) was used to investigate the phase morphology due to the polymerization induced phase separation process. Specimens were put under a Cathode (typically Gold), and the bombardment of the gold with Argon erodes the target material onto the surface of the specimens. An accelerating voltage at 15 KV was applied to accomplish a designed magnification. Micrographs were captured with a scan speed at 35 seconds.

RESULTS AND DISCUSSION

Thermal Properties

The thermal properties of the PCL based composite were studied by DSC method. The second heating DSC trace is shown in Fig. 3. It shows a melting transition of "soft" phase at 53°C followed by a step transition at 138.5°C. These two transitions correspond to the melting of PCL and glass transition of the epoxy network, respectively. It is interesting to note that the PCL phase has a lower melting temperature than the one provided by the vendor. This might be due to the lower degree of crystallinity in PCL based composite, which was fabricated via PIPS. As reported in a previous work, a phase melting point at 58°C was observed [18]. The PCL particles were mixed and distributed over the epoxy matrix for crack self-healing purpose. The fabrication process did not change the molecular structure. However, in this study, the fabrication process involves polymerization, during which the molecular structure of PCL could be affected.

Morphology Characterization

In this study, PCL particles were melted firstly while mixing with liquid resin. Curing agent was added to the mixture after that. The cure reaction leaded to a molecular weight increase and phase separation [30]. The original fracture surfaces from tested Arcan specimens were investigated. The two-phase morphology of surfaces is presented in Fig. 4. As can be seen, the connected-globule structure exists on the investigated surfaces. Fine globules of a few micrometers were formed and interconnected. As measured from the microscopic results, the

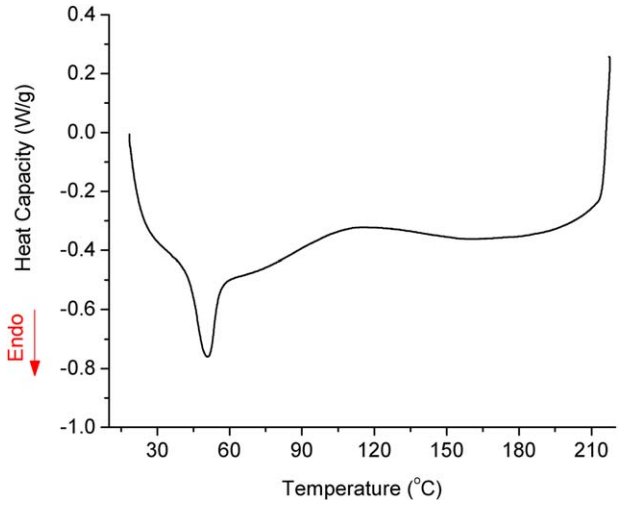

FIG. 3. DSC results for the PCL based polymer composite specimen. [Color figure can be viewed at wileyonlinelibrary.com]

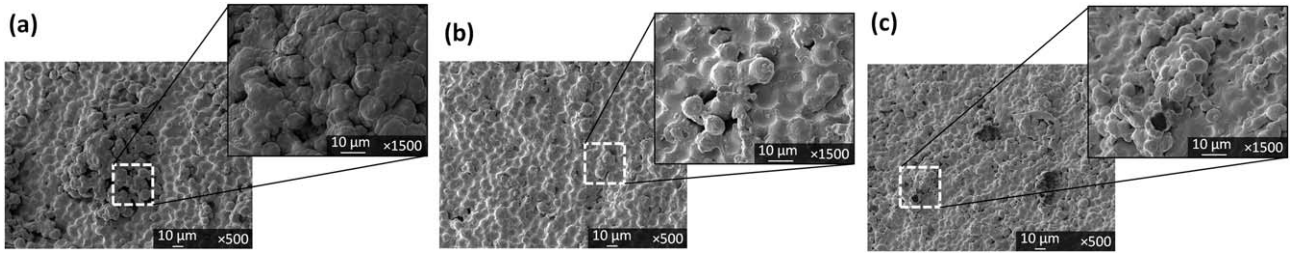

FIG. 4. SEM characterization on fracture surfaces: (a) 10% PCL, (b) 12% PCL, and (c) 14% PCL.

sizes of the globules are from 6.89 to 10.37 μm for 10% PCL sample, from 6.63 to 9.33 μm for 12% PCL sample, and 4.61 to 8.19 μm for 14% PCL sample. It is clear that the average size decreases as the amount of PCL increasing. In addition, the globules are uniformly distributed across the fracture surfaces. This is because the phase separation increases due to the increase of the PCL amount [31].

Shape Memory Characterization

The purpose of this test is to verify the shape memory performance of the fabricated specimens in terms of stress and strain recovery. Both the stress recovery and strain recovery tests were conducted at the temperature of 80°C. It is worth noting that the specimen, with an amount of 12% PBV PCL, was broken during the stress recovering process if programmed over a prestrain = 0.14. The maximum recovered stress was 0.57 MPa. Obviously the recovered stress caused the breaking of test sample. Therefore, in order to investigate the effect of PCL amount on shape memory performance, all specimens were programmed at a prestrain = 0.13. Figure 5 shows the recovered compression stresses, which stabilized within 6 minutes at 0.35 MPa, 0.39 MPa, and 0.42 MPa for 10%, 12%, and 14% PCL specimens, respectively. It also shows that the recovered stress increases as the PCL increases, due to the shape memory effect of PCL.

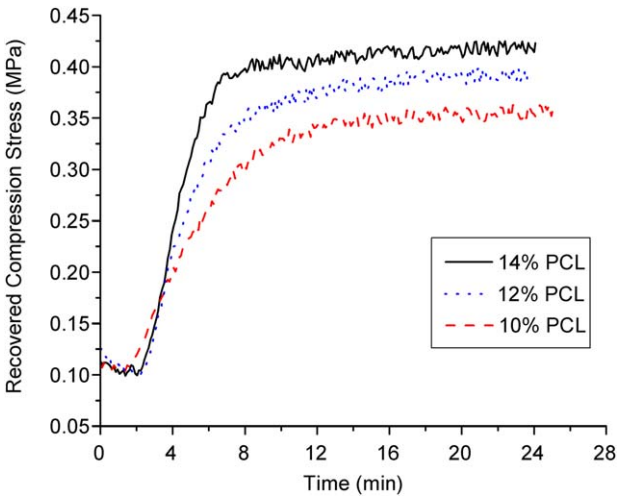

FIG. 5. Stress recoveries of polymer composite specimens. [Color figure can be viewed at wileyonlinelibrary.com]

Results from our experiments show that, if the PCL amount is higher than 14%, the mixture of PCL and epoxy resin becomes very viscous once cools down to a temperature lower than 53°C. Adding curing agent did not help the flow of the mixture. Viscous mixture makes the fabrication process difficult; while incomplete polymerization makes the sample quality poor. To have good quality specimens, the maximum percentage by volume of PCL is 14%. It is believed that the larger programming prestrain means larger recovered stress [18]. Therefore, in order to have a larger recovered stress, for example larger than 0.42 MPa, the specimen has to be programmed with a larger prestrain, which can be obtained at a higher temperature (i.e., higher than 80°C).

The strain recovery ratio η was calculated from recovered strain over temporary deformed strain

$$\eta = \epsilon_r / \epsilon_d = (l_r - l_f)/(l_o - l_f) \quad (1)$$

where $_r$ is the recovered strain, $_d$ is the programmed strain, l_r is the specimen length after recovery, l_f is the specimen length at the end of programming process, and l_o is the original specimen length. As shown in Table 1, it is clear that higher PCL amount leads to higher strain recovery ratio, which is in agreement with the stress recovery results. This is because the potential of strain recovery was converted to force due to the constraint boundaries during stress recovery [32]. The maximum ratio is 78%, indicating the temporary shape was not fully recovered. This is due to the non-shape memory hard phase component of the epoxy network [33, 34]. As being discussed in Fig. 3, the glass transition temperature of the hard phase is about 138.5°C. At 80°C, the temporary shape was stilled "locked" by the epoxy networks.

TABLE 1. Shape recovery performance of PCL based composite specimens.

Specimen entry	Strain recovery ratio (%)	Maximum stress recovery (MPa)
PCL-10% PBV	47.40	0.35
PCL-12% PBV	69.12	0.39
PCL-14% PBV	78.10	0.42

DOI 10.1002/pc

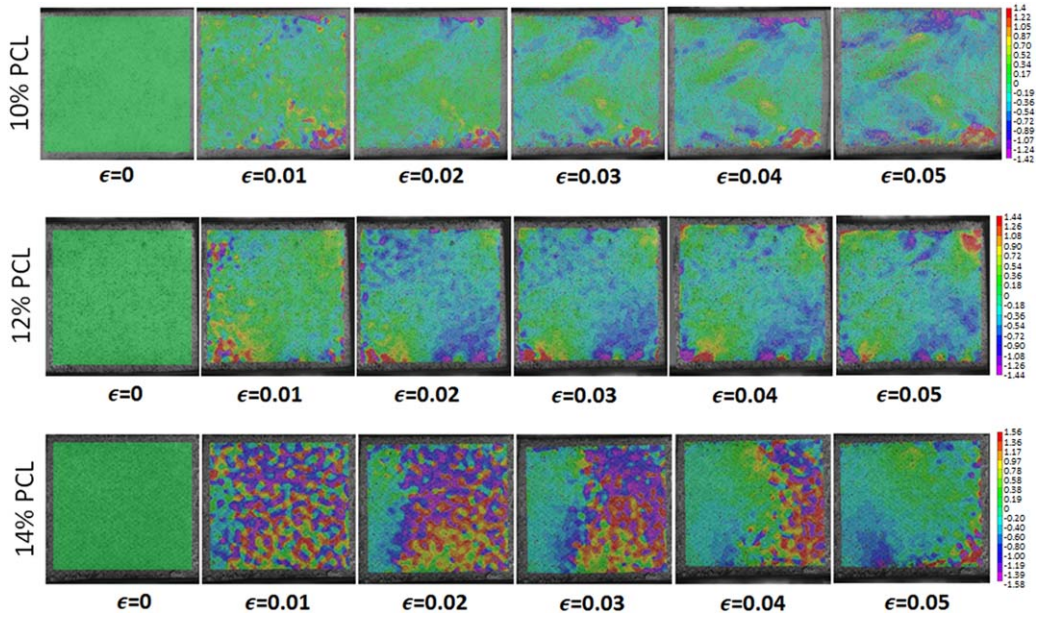

FIG. 6. The DIC full-field strain information for the composite specimens. [Color figure can be viewed at wileyonlinelibrary.com]

Compression Properties

The DIC has been widely used on structural materials to obtain the full-field strain distribution to sub-pixel accuracy [35, 36], even on polymer composites [37]. In this study, the purpose of using DIC is to quantitatively determine the deformation field and characterize the deformation mechanism of various phases. Figure 6 shows the full-field strain information for different specimens under compression loading. Pictures taken at =0 are the reference images. The rest images were taken at =0.01, =0.02, =0.03, =0.04, and =0.05, respectively. Due to the limited imaging rate (1 image per 5 seconds) and rapid deformation at large strain, the VIC-2D could not precisely track the speckle pattern at larger strains.

The effect of PCL content on polymerization-induced phase separation (PIPS) could not be clearly seen from the morphology characterization (see Fig. 4). But the effect can be articulated from DIC strain field analysis. As shown in Fig. 6, for specimen with 10% PCL, the strain field is uniformly distributed until =0.02. After that the strain becomes concentrated. For specimen with 12% PCL, the strain field is uniformly distributed until =0.01. The strain field is linearly distributed for these two specimens while loading from =0.01 to =0.05, which means larger deformation leads to higher strain concentration. However, nonlinear strain field distribution can be observed for specimen with 14% PCL. Strain concentration occurs at =0.01. After that, the concentration shifts to the right hand side from =0.02 to =0.04 and becomes inconspicuous at =0.05. This phenomenon is due to the misalignment of different phases under loading [38].

Specimens were tested under compression at room temperature. Figure 7 shows the typical compression performance in terms of PCL volume fractions, from which it is clear to see that higher amount of PCL leads to better compression strength. According to the DIC and compression results, mechanical properties of the specimens were determined in Table 2. Observations include: (1) Both the fracture strain and maximum compressive stress increase as the amount of PCL increases. It indicates, within the allowable limit, that adding PCL improves the compression toughness. (2) The specimen with 12% PCL has the highest Young's modulus, while the specimen with 10% PCL has lowest Young's modulus. It is worth noting that,

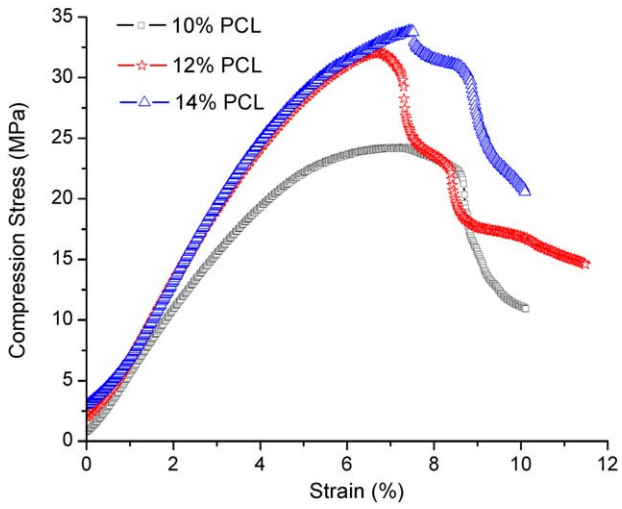

FIG. 7. Typical compression results for specimens in terms of different amount of PCL. [Color figure can be viewed at wileyonlinelibrary.com]

TABLE 2. Mechanical properties of PCL based polymer composites.

Specimen entry	Fracture strain (%)	Maximum compressive stress (MPa)	Young's modulus (MPa)	Poisson's ratio
PCL-10% PBV	6.11 ± 0.70	24.15 ± 0.02	542 ± 19	0.45 ± 0.03
PCL-12% PBV	6.45 ± 0.48	28.95 ± 2.61	657 ± 21	0.47 ± 0.02
PCL-14% PBV	7.08 ± 0.66	30.36 ± 2.96	583 ± 17	0.44 ± 0.02

with 14% PCL, the mixture became very viscous during the fabrication process as compared with the other two mixtures. Such phenomenon might contribute to the decrease in the specimen stiffness. (3) Poisson's ratio of the PCL based composite specimen is about 0.45. The data from DIC were used to calculate the Poisson's ratio.

Fracture Toughness

Fracture toughness of the composites were obtained from the Arcan tests as

$$K_{IC} = \left(P_c\sqrt{\pi a}/2Wt\right)\cos(\theta) f_I(a/W) \quad (2)$$

$$K_{IIC} = \left(P_c\sqrt{\pi a}/2Wt\right)\sin(\theta) f_{II}(a/W) \quad (3)$$

here K_{IC} and K_{IIC} are critical stress intensity factors for mode I and mode II [23, 39]. P_c is the critical load on the load-displacement curve. Figure 8 shows a typical load-displacement curve for specimens in terms of different amount of PCL under mode I loading. There is a sharp peak on each curve. The peak value is the critical load that was used to determine the critical stress intensity factor. θ is the loading angle. $f_I(a/W)$ and $f_{II}(a/W)$ are geometrical factors. Since solutions were not available in the reported literatures for the finite geometry function, it was numerically determined using finite element models to compare stress intensity factors for angles $\theta = 0°$ and $\theta = 90°$. When developing a finite element model, 3D curvature-based mesh element was chosen to discretize the Arcan specimen.

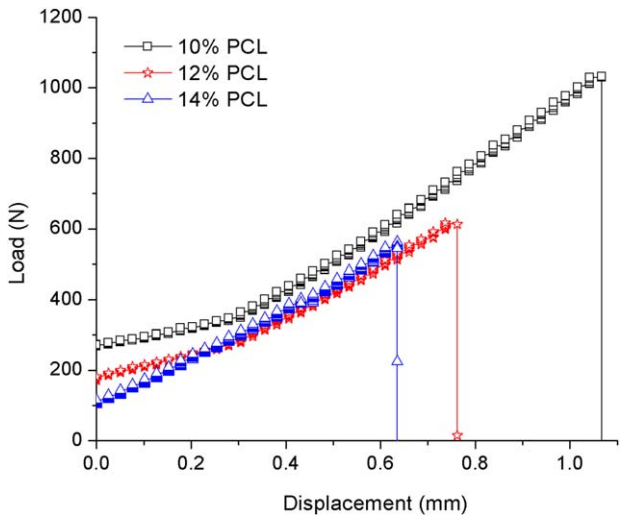

FIG. 8. Typical load-displacement curve for specimens in terms of different amount of PCL under mode I loading. [Color figure can be viewed at wileyonlinelibrary.com]

By using the finite element method, it is necessary to isolate each variable. Only in this case it can determine how the finite dimension affects the critical stress intensity factor. As pointed out by Riggenbach [39], a set of models should be created varying only the chosen dimension. In this study, the primary dimension varied is the pre-crack length (a). In order to limit the number of models and data generated, the meshing element size was chosen as 1.27 mm and the ratio of investigated was 0.2, 0.3, 0.4, 0.5, 0.6, 0.7, and 0.8 according to the realistic configurations. A set of critical stress intensity factors resulted from the finite element models were eventually obtained. The data were normalized according to the *Eqs. 2* and *3* to obtain the geometrical factors. OriginPro 8 was used for data fitting since it has a large internal database of functions to allow users to choose the best function for their applications. The geometrical factors are shown in Fig. 9, from which the geometrical factor functions for Mode I and Mode II were obtained through curve fitting:

$$f_I(a/W) = 0.97 + 32.39(a/W) - 141.43(a/W)^2 + 266.54(a/W)^3 - 131.85(a/W)^4 \quad (4)$$

$$f_{II}(a/W) = -17.20 + 409.94\left(\frac{a}{W}\right) - 1433.67\left(\frac{a}{W}\right)^2 + 1925.74\left(\frac{a}{W}\right)^3 - 699.41\left(\frac{a}{W}\right)^4. \quad (5)$$

The critical stress intensity factors K_{IC} and K_{IIC} could be calculated when plugging *Eqs. 4* and *5* into *Eqs. 2* and *3*. Keep in mind that K_{IC} is determined at $\theta = 0°$ (see Fig. 9a) while K_{IIC} is determined at $\theta = 90°$ (see Fig. 9b). The ASTM D5045-99 was used to verify the geometry factors and critical stress intensity factor determined from Arcan tests results. The standard method is designed to characterize the toughness of plastics in terms of the critical stress intensity factor, K_{IC}, and the energy per unit area of crack surface or critical strain energy release rate, GIC, at fracture initiation. The geometrical factor obtained computationally was verified by resorting to a comparison with geometrical factor provided by the ASTM D5045, as shown in Fig. 10(a). Since the ASTM D5045 only provides the geometrical factor values within an a/W ratio range from 0.45 to 0.55, the Fig. 10(a) only presents a short curve of geometrical factor according to the standard method ASTM D5045. In order to have a

 DOI 10.1002/pc

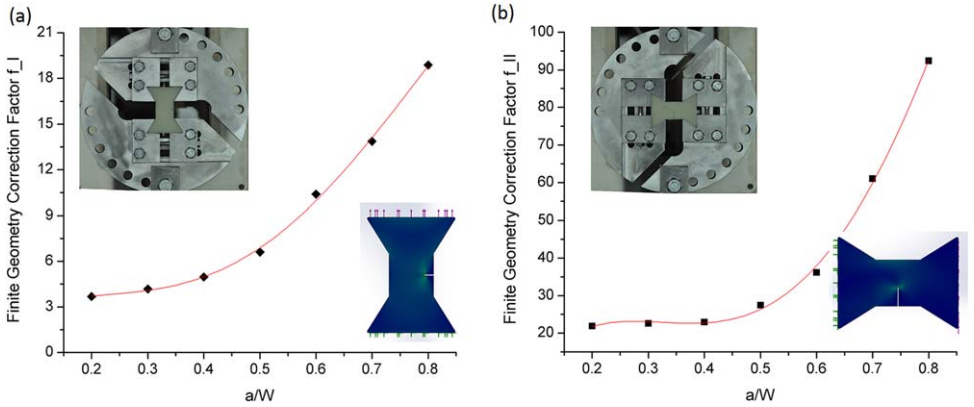

FIG. 9. Geometrical factors from varied a/W ratios: (a) at $\theta = 0°$; and (b) at $\theta = 90°$. [Color figure can be viewed at wileyonlinelibrary.com]

comparison with critical stress intensity factor K_{IC}, 3-point bending tests were conducted on single-edge-notch bending (SENB) samples according to the ASTM D5045. The K_{IC} of SENB specimens was calculated based on the experimentally obtained peak bending fracture load and specimen geometry sizes. The comparison is shown Fig. 10(b). What can be observed include: (1) both mode I geometry factor and critical stress intensity factor according to Arcan loading fixture have a similar trend as those factors obtained according to the ASTM D5045 and (2) as compared, the values of those factors obtained from Arcan specimens are smaller, indicating the Arcan loading fixture is more conservative than the standard 3-point bending test fixture.

It was found that, with crack length ratio a/W=0.2, no effective experimental data were obtained for determining K_{IIC}. In order to have valid experimental data, there is a need to investigate the fracture toughness at different crack length ratios. What can be seen from Fig. 9 is that the geometrical factors increase fast once the crack length ratio achieves 0.6. Therefore, the fracture toughness was experimentally investigated at ratios of 0.2, 0.4, and 0.6. The effect of crack length on critical stress intensity factors is shown in Fig. 11. The dash line is the trendline showing the tendency of toughness change along with the increase of crack length. It is clear that the increase of crack length ratio does not change the critical stress intensity factors, which is in agreement with what has been reported from the usage of Arcan test fixture [27, 40]. The critical stress intensity factors are presented in Table 3, from which it can be seen: (1) K_{IC} decreases along with the increase in PCL content and (2) K_{IIC} decreases first then increases as the amount of PCL increases from 10% to 14%. Furthermore, it indicates that adding PCL can improve the shear resistance, for example, the K_{IIC} is larger than K_{IC} for specimen with 12% PCL and it becomes three times of K_{IC} when the PCL is 14%.

During the fracture tests, the loading angles included 0°, 30°, 45°, 60°, 75°, and 90° (refer to Fig. 2). The critical stress intensity factors K_{IC} and K_{IIC} at different angles could be calculated when plugging *Eqs. 4* and *5* into *Eqs. 2* and *3*. Figure 12 shows the effect of loading angles on fracture toughness. After curve fitting, it roughly shows that, for specimens with 10% and 12% PCL, Mode I fracture is dominant when loading angle is smaller than 45°,

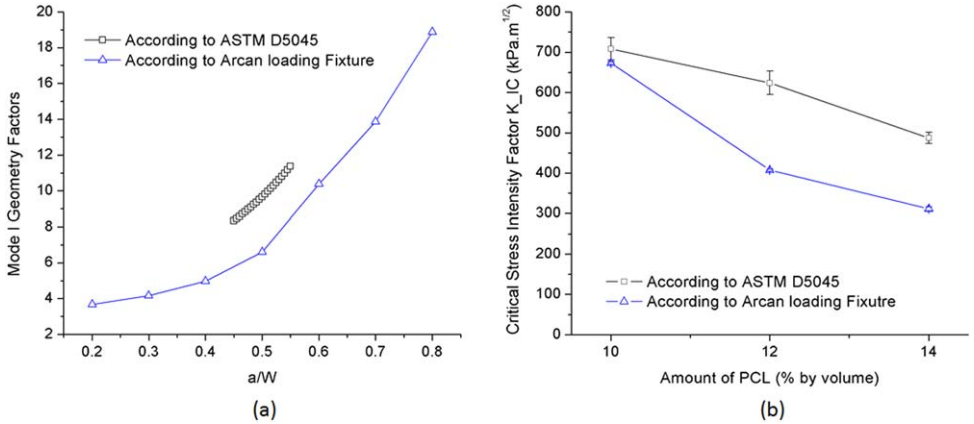

FIG. 10. Comparisons of mode I geometry factors (a) and mode I critical stress intensity factors (b) according to the ASTM D5045 and Arcan loading fixture. [Color figure can be viewed at wileyonlinelibrary.com]

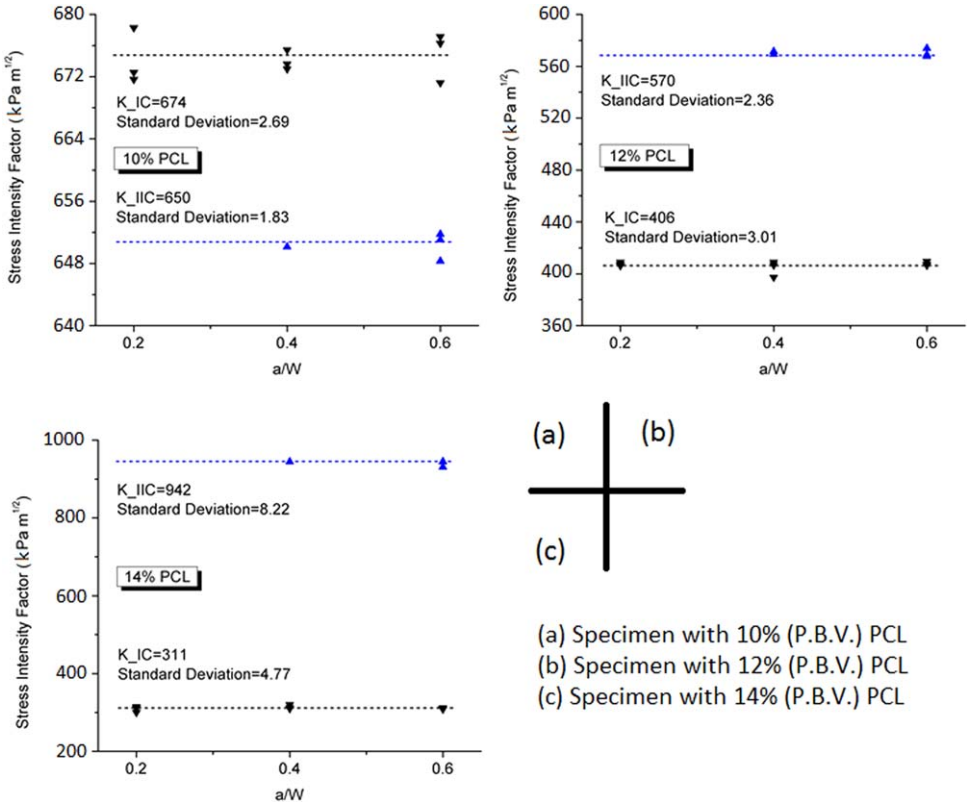

FIG. 11. The effect of crack lengths on fracture toughness at $\theta = 0°$ and $\theta = 90°$. [Color figure can be viewed at wileyonlinelibrary.com]

while on the other hand Mode II fracture is dominant. However, Mode I fracture is dominant if the angle is smaller than 53° for specimen with 14% PCL. This change is of interest, which indicates that the increase in PCL content not only affects shape memory performance and compression strength, but also the fracture behavior.

In a generally proposed form, the mixed mode fracture behavior is represented by $(K_I/K_{IC})^2+(K_{II}/K_{IIC})^2=1$. [23, 27, 28]. Using the average values of K_{IC} and K_{IIC} in Table 3, the mixed mode fracture criteria for specimens with 10% PCL, 12% PCL, and 14% PCL were respectively determined as:

$$(K_I/674)^2+(K_{II}/650)^2=1 \quad (6)$$

$$(K_I/406)^2+(K_{II}/570)^2=1 \quad (7)$$

$$(K_I/311)^2+(K_{II}/944)^2=1. \quad (8)$$

The relationships between mixed-mode critical stress intensity factors and loading angles are presented in Fig. 13. As mentioned earlier, no effective experimental data were obtained for K_{IIC} at crack length ratio 0.2. But there are sufficient data for both K_{IC} and K_{IIC} if the ratio is 0.6 (see Fig. 9). Hence, the relationships shown in Fig. 13 were derived at the crack length ratio of 0.6. As discussed earlier, the change of crack length does not have an impact on the stress intensity factors. As a result, the derived relationships shall not be affected by the crack length ratio either. It can be observed that: (1) the increase in PCL content leads to a decrease in K_{IC} but an overall increase in K_{IIC} (see Fig. 13a); (2) the mode I critical stress intensity factor decreases fast with increase in loading angle for specimen with 10% PCL, but mode II critical stress intensity factor decreases slowly for loading angles larger than about 60° (see Fig. 13b); (3) the change of both mode I and mode II critical stress intensity factors behaves similar to the change of loading angles for specimen with 12% PCL, i.e., loading angle has similar effect on both tensile and shear fracture behavior (see Fig. 13c); and (4) in a completely different way, the mode I critical stress intensity factor remains almost constant for loading angles smaller than 45° for specimen with 14% PCL, but mode II critical stress intensity factor decreases rapidly with increase in loading angles (see Fig. 13d).

TABLE 3. Critical stress intensity factor of PCL based polymer composites.

Critical stress intensity factor (kPa$\sqrt{m}$)	PCL-10% PBV	PCL-12% PBV	PCL-14% PBV
K_{IC}	674	406	311
K_{IIC}	650	570	944

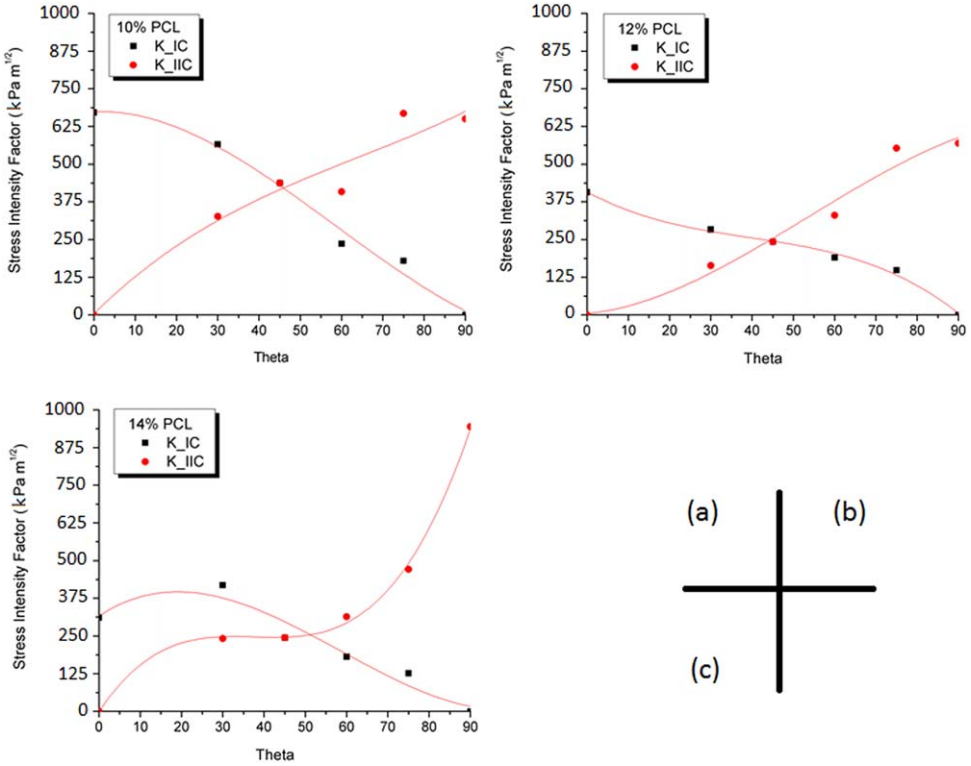

FIG. 12. The effect of loading angles on specimen fracture toughness with =0.6. [Color figure can be viewed at wileyonlinelibrary.com]

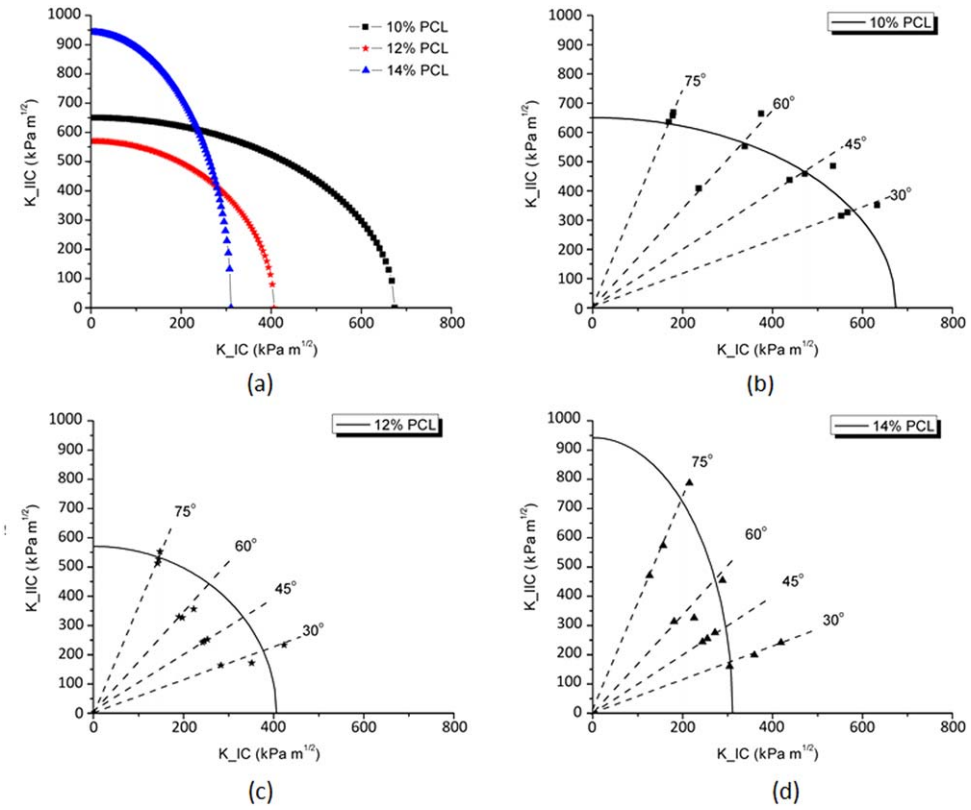

FIG. 13. Predictions of mixed mode fracture criteria of composite specimen with a/W = 0.6. [Color figure can be viewed at wileyonlinelibrary.com]

CONCLUSIONS

Fracture behavior for PCL based polymer composite materials has been investigated using Arcan specimens. Shape memory performance of specimens fabricated by PIPS process was evaluated through stress and strain recovery tests. The mechanical properties, including Young's modulus and Poisson's ratio, were determined through compression test along with DIC technique. In order to investigate the fracture toughness for the shape memory composite material, geometrical factors were determined through finite element method while kept varying only the pre-crack length. The critical stress intensity factors were determined to be 674 kPa$\sqrt{m}$ and 650 kPa$\sqrt{m}$ for specimen with 10% PCL, 406 kPa$\sqrt{m}$ and 570 kPa$\sqrt{m}$ for specimen with 12% PCL, and 311 kPa$\sqrt{m}$ and 944 kPa$\sqrt{m}$ for specimen with 14% CPL for the mode I and mode II, respectively. A distinct phenomenon was observed for fracture behavior if the amount of PCL is over 14%.

REFERENCES

1. Q. Zhao, H.J. Qi, and T. Xie, *Prog. Polym. Sci.*, **49–50**, 79 (2015).
2. M.D. Hager, S. Bode, C. Weber, and U.S. Schubert, *Prog. Polym. Sci.*, **49–50**, 3 (2015).
3. P. Zhang and G. Li, *Prog. Polym. Sci.*, **57**, 32 (2016).
4. J. Hu, Y. Zhu, H. Huang, and J. Lu, *Prog. Polym. Sci.*, **37**, 1720 (2012).
5. J.S. Leng, X. Lan, Y.J. Liu, and S.Y. Du, *Prog. Mater. Sci.*, **56**, 1077 (2011).
6. M. Behl and A. Lendlein, *Mater. Today*, **10**, 20 (2007).
7. C. Zhang, Y. Xia, R. Chen, S. Huh, P.A. Johnston, and M.R. Kessler, *Green Chem.*, **15**, 1477 (2013).
8. C. Zhang, R. Ding, and M.R. Kessler, *Macromol. Rapid Commun.*, **35**, 1068 (2014).
9. G. Li, *Self-Healing Composites: Shape Memory Polymer Based Structures*. John Wiley & Sons Ltd, West Sussex, United Kingdom (2014).
10. G. Li and D. Nettles, *Polymer*, **51**, 755 (2010).
11. G. Li and N. Uppu, *Compos. Sci. Technol.*, **70**, 1419 (2010).
12. G. Li, H. Meng, and J. Hu, *J. R. Soc. Interface*, **9**, 3279 (2012).
13. P. Zhang and G. Li, *Polymer*, **64**, 29 (2015).
14. G. Li and M. John, *Compos. Sci. Technol.*, **68**, 3337 (2008).
15. J. Nji and G. Li, *Smart Mater. Struct.*, **19**, 035007 (2010).
16. M. John and G. Li, *Smart Mater. Struct.*, **19**, 075013 (2010).
17. J. Nji and G. Li, *Polymer*, **51**, 6021 (2010).
18. G. Li and P. Zhang, *Polymer*, **54**, 5075 (2013).
19. G. Li, O. Ajisafe, and H. Meng, *Polymer*, **54**, 920 (2013).
20. E.N. Brown, N.R. Sottos, and S.R. White, *Exp. Mech.*, **42**, 372 (2002).
21. E.N. Brown, *J. Strain Anal. Eng. Des.*, **46**, 167 (2011).
22. S. Neuser, V. Michaud, and S.R. White, *Polymer*, **53**, 370 (2012).
23. N. Choupani, *Mater. Sci. Eng. A*, **478**, 229 (2008).
24. M. Nikbakht and N. Choupani, *J. Mater. Sci.*, **44**, 3428 (2009).
25. F.J. Chaves, L.F.M. Da Silva, M.F.S.F. De Moura, D.A. Dillard, and V.H.C. Esteves, *J. Adhes.*, **90**, 955 (2014).
26. M. Arcan, Z. Hashin, and A. Voloshin, *Exp. Mech.*, **18**, 141 (1978).
27. R.A. Jurf and R.B. Pipes, *J. Compos. Mater.*, **16**, 386 (1982).
28. S.H. Yoon and C.S. Hong, *Exp. Mech.*, **30**, 234 (1990).
29. A.H. Torbati, H.B. Nejad, M. Ponce, J.P. Sutton, and P.T. Mather, *Soft Matter*, **10**, 3112 (2014).
30. T. Inoue, *Prog. Polym. Sci.*, **20**, 119 (1995).
31. H.M. Jeong, J.H. Song, S.Y. Lee, and B.K. Kim, *J. Mater. Sci.*, **36**, 5457 (2001).
32. H. Meng and G. Li, *Polymer*, **54**, 2199 (2013).
33. C.L. Lewis and E.M. Dell, *J. Polym. Sci. B Polym. Phys.*, **54**, 1340 (2016).
34. W. Wang, Y. Liu, and J. Leng, *Coord. Chem. Rev.*, **320–321**, 38 (2016).
35. K. Gall, M.L. Dunn, Y. Liu, D. Finch, M. Lake, and N.A. Munshi, *Acta Mater.*, **50**, 5115 (2002).
36. B. Pan, K. Qian, H. Xie, and A. Asundi, *Meas. Sci. Technol.*, **20**, 062001 (2009).
37. M. Jerabek, Z. Major, and R.W. Lang, *Polym. Test.*, **29**, 407 (2010).
38. S.R. Heinz and J.S. Wiggins, *Polym. Test.*, **29**, 925 (2010).
39. K.R. Riggenbach, "Finite Geometry Correction Factors for the Stress Field and Stress Intensities at Transverse Fillet Welds," Dissertation, Case Western Reserve University (2012).
40. L. Banks-Sills, M. Arcan, and Y. Bortman, *Eng. Fract. Mech.*, **20**, 145 (1984).